Supporting Information

Searching for Simple β-$A^{I}M^{III}O_2$-type Intrinsic Ferroelectric Semiconductors with Simultaneous Robust Built-in Electric Field and Full-Spectrum Absorption for Superior Photocatalyst

Ruichen Wang, [abc] Lanlan Xu, [*cd] Qingshi Liu, [ce] Qiang Shi, [d] Xiaojuan Liu, [*abc]

[a] *School of Rare Earths，University of Science and Technology of China, Hefei, Anhui 230026, China.*

[b] *Ganjiang Innovation Academy, Chinese Academy of Sciences, Ganzhou, 341000, China*

[c] *State Key Laboratory of Rare Earth Resource Utilization, Changchun Institute of Applied Chemistry, Chinese Academy of Sciences, Changchun, 130022, China*

[d] *State Key Laboratory of Polymer Chemistry and Physics, Changchun Institute of Applied Chemistry, Chinese Academy of Sciences, Changchun, 130022, China*

[e] *University of Science and Technology of China, Hefei, Anhui 230026, China*

In the linear deformation range of the material (under small strain), the stresses and strains of the system satisfy Hooke's law,

$$\sigma_i = \sum_{j=1}^{\sigma} C_{ij}\varepsilon_j \tag{1}$$

where σ_i and ε_i correspond stress as well as strain apart. C_{ij} is the elastic stiffness constant, where $1 \leq i \leq 6$, that is, the strain and stress have respectively six independent components. The strain energy of the system after applying strain can be obtained by Taylor series expansion and second-order approximation according to strain tensor:

$$\Delta E\left(V,\{\varepsilon_i\}\right) = E\left(V-\{\varepsilon_i\}\right) - E\left(V_0,0\right) = \frac{V_0}{2}\sum_{i,j=1} C_{ij}\varepsilon_j\varepsilon_i \tag{2}$$

where E (V, [1]) is the total energy after applying strain and E (V_0, 0) is the energy of the ground state configuration. The change of the total energy relative to the ground state energy (strain energy) is calculated, and the quadratic polynomial is fitted by **Eq. (2)**, where the coefficient of the quadratic polynomial is a certain elastic constant or a combination of elastic constants of the crystal. The number of independent elastic constants depends on the symmetry of the crystal. Lower symmetry means more independent elastic constants. In this paper, all systems belong to orthorhombic crystals, which have nine independent elastic constants.[2] The stiffness matrix has the following form:

$$C_{ortho} = \begin{pmatrix} C_{11} & C_{12} & C_{13} & & & \\ \cdot & C_{22} & C_{23} & & C_{55} & \\ \cdot & \cdot & C_{33} & C_{44} & & C_{66} \end{pmatrix} \tag{3}$$

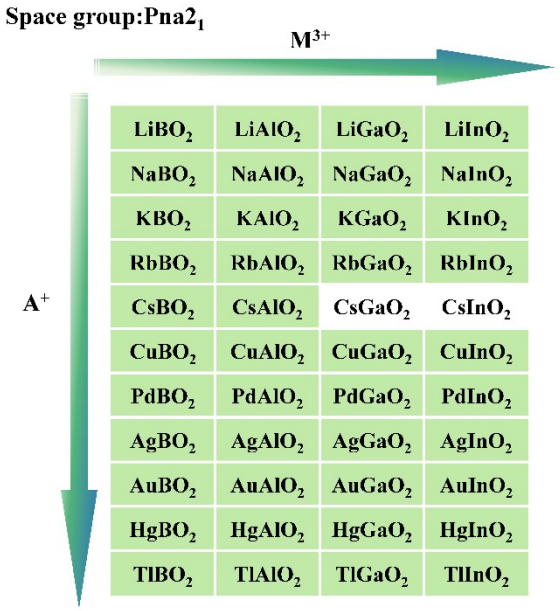

Figure S1. The schematic diagram of structural relaxation screening. From 44 crystal databases, 42 structurally stable systems were selected by preliminary structural optimization.

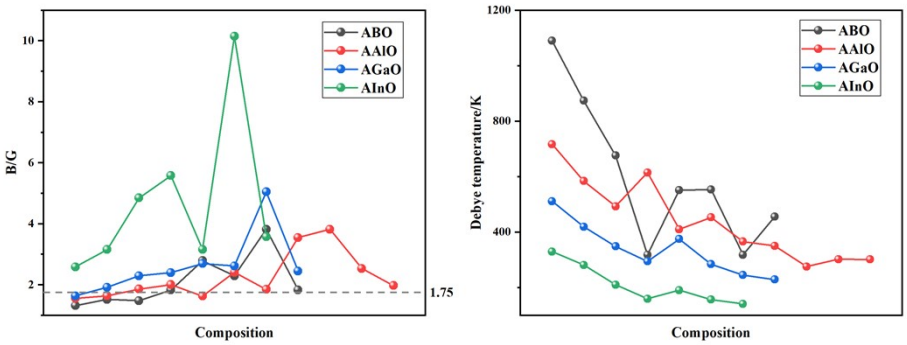

Figure S2. The calculated B/G and Debye temperature θ_D (K) images.

Pugh's empirical relation says that the ratio of the bulk modulus to shear modulus can be used to distinguish ductile and brittle materials based on a critical value of 1.75. [3]From Figure S7 shows, most of the systems have B/G values greater than 1.75, which are ductile materials. Only a few, such as β-$LiBO_2$, β-$LiAlO_2$, β-$LiGaO_2$ and β-$NaBO_2$, are brittle materials. Finally, Debye temperature (θ_D) corresponds to the highest frequency of lattice vibration, and it's actually a reflection of the strongest bond of crystal binding. Debye temperature varies with different materials. The stronger the bonding force between the atoms, the higher the Debye temperature. Our work reveals that Debye temperature roughly decreases with the increase of the M-site cation size.

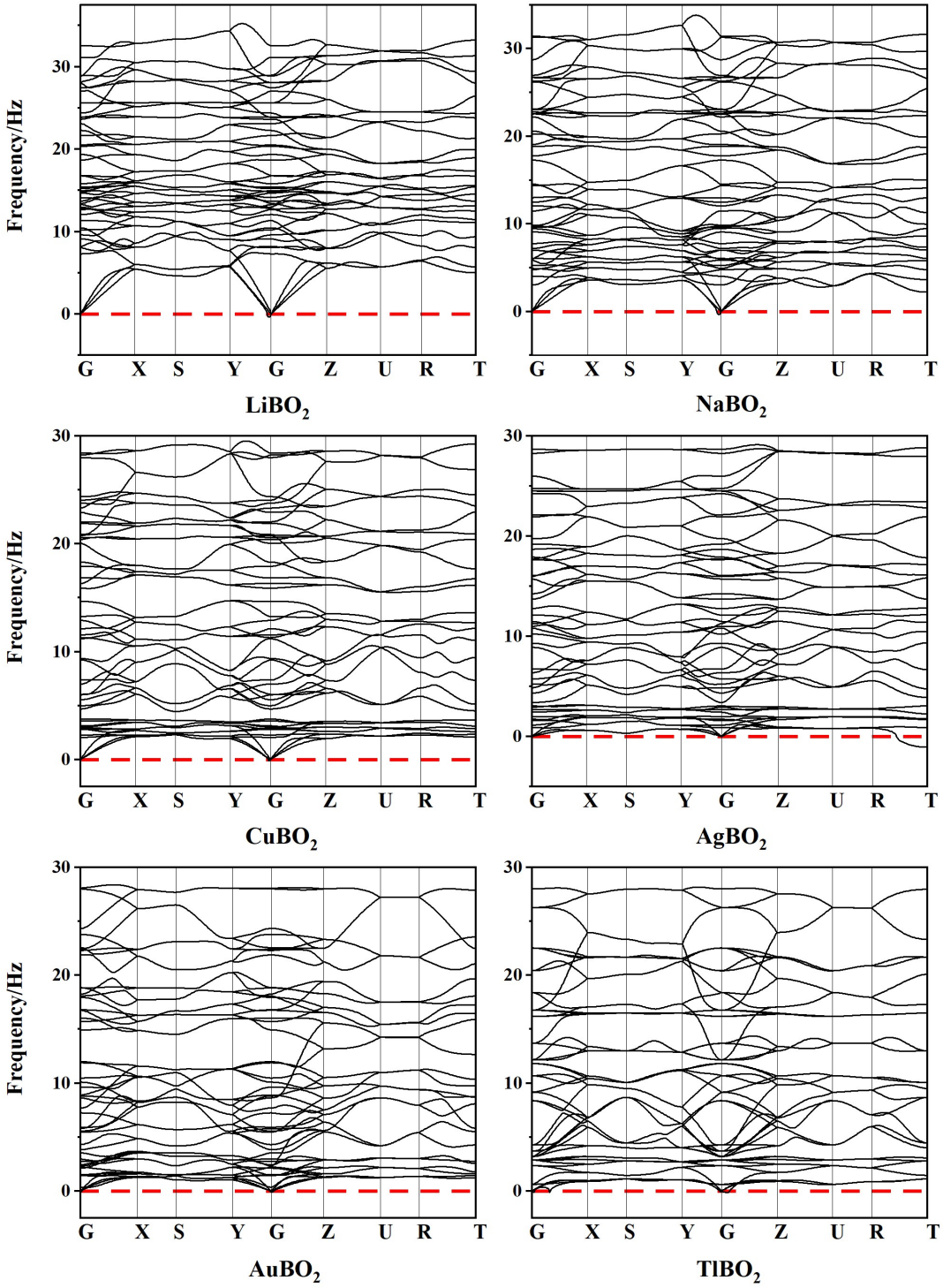

Figure S3 (a). The phonon spectrum of β-ABO_2 series system. All β-ABO_2 series oxides are thermodynamically stable.

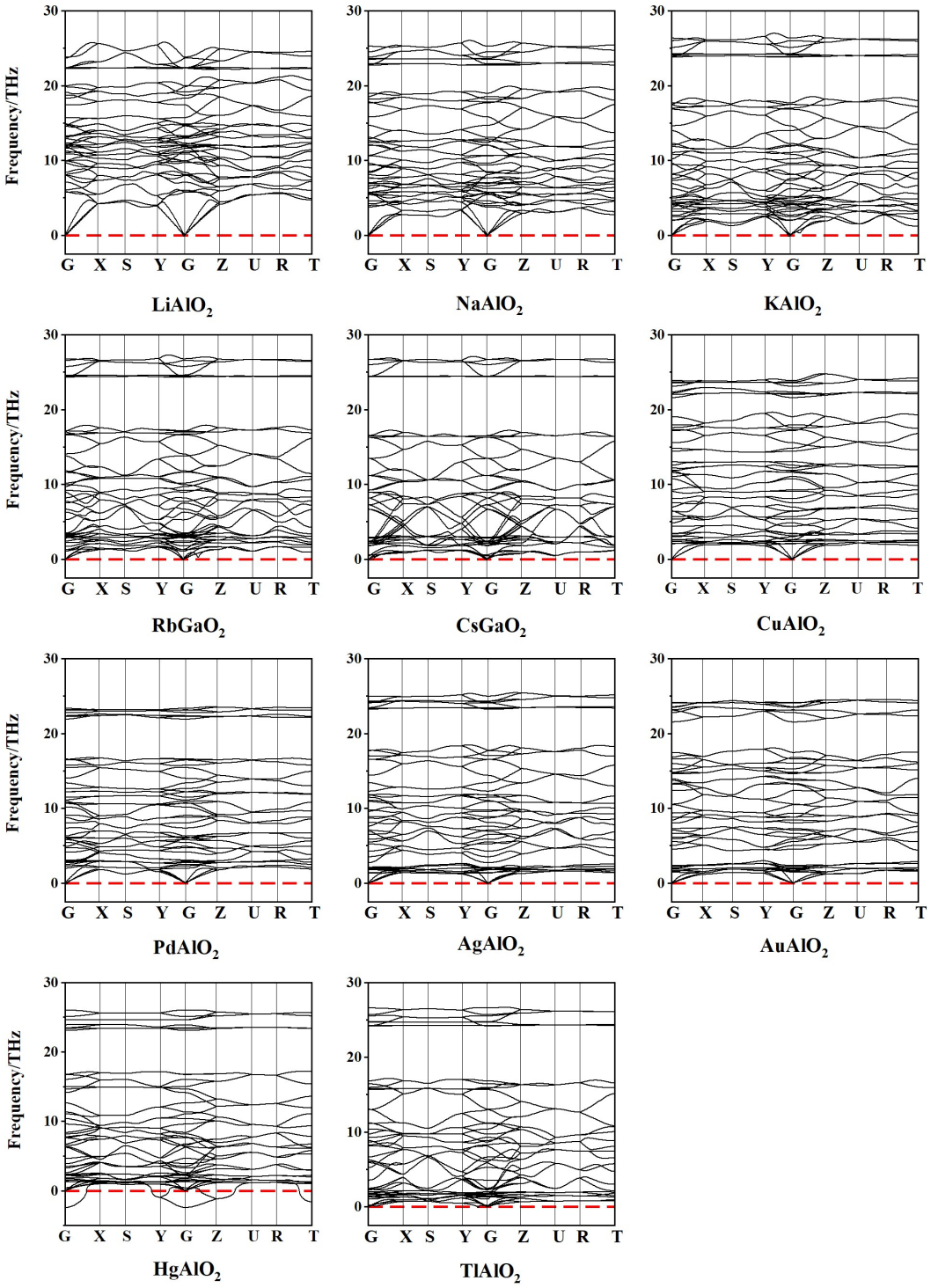

Figure S3 (b). The phonon spectrum of β-$AAlO_2$ series system. Among the β-$AAlO_2$ oxides, only the β-$HgAlO_2$ has virtual frequency and is thermodynamically unstable.

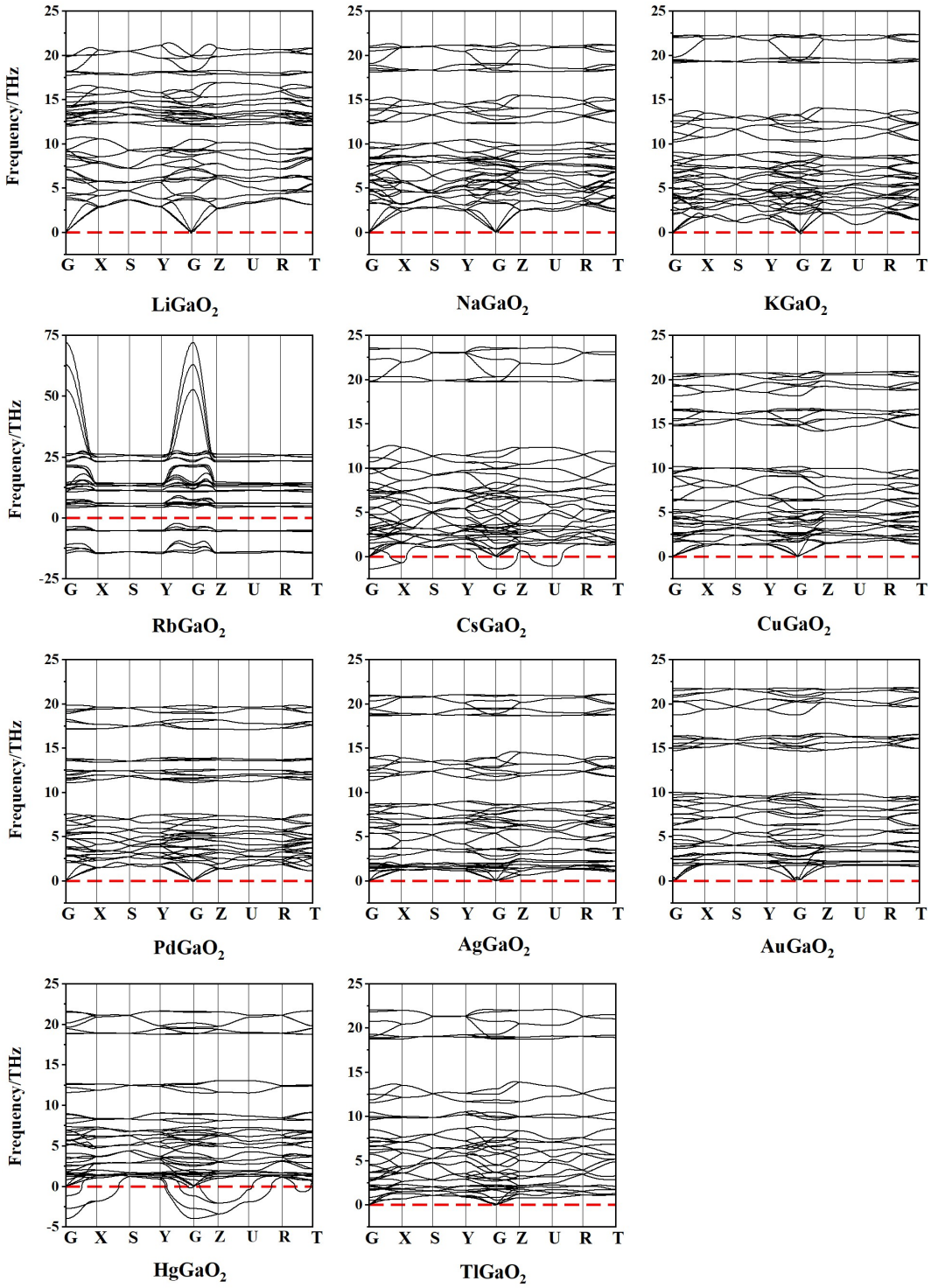

Figure S3 (c). The phonon spectrum of β-$AGaO_2$ series system. Among the β-$AGaO_2$ oxides, the β-$RbGaO_2$, β-$CsGaO_2$ and β-$HgGaO_2$ have virtual frequency and are thermodynamically unstable.

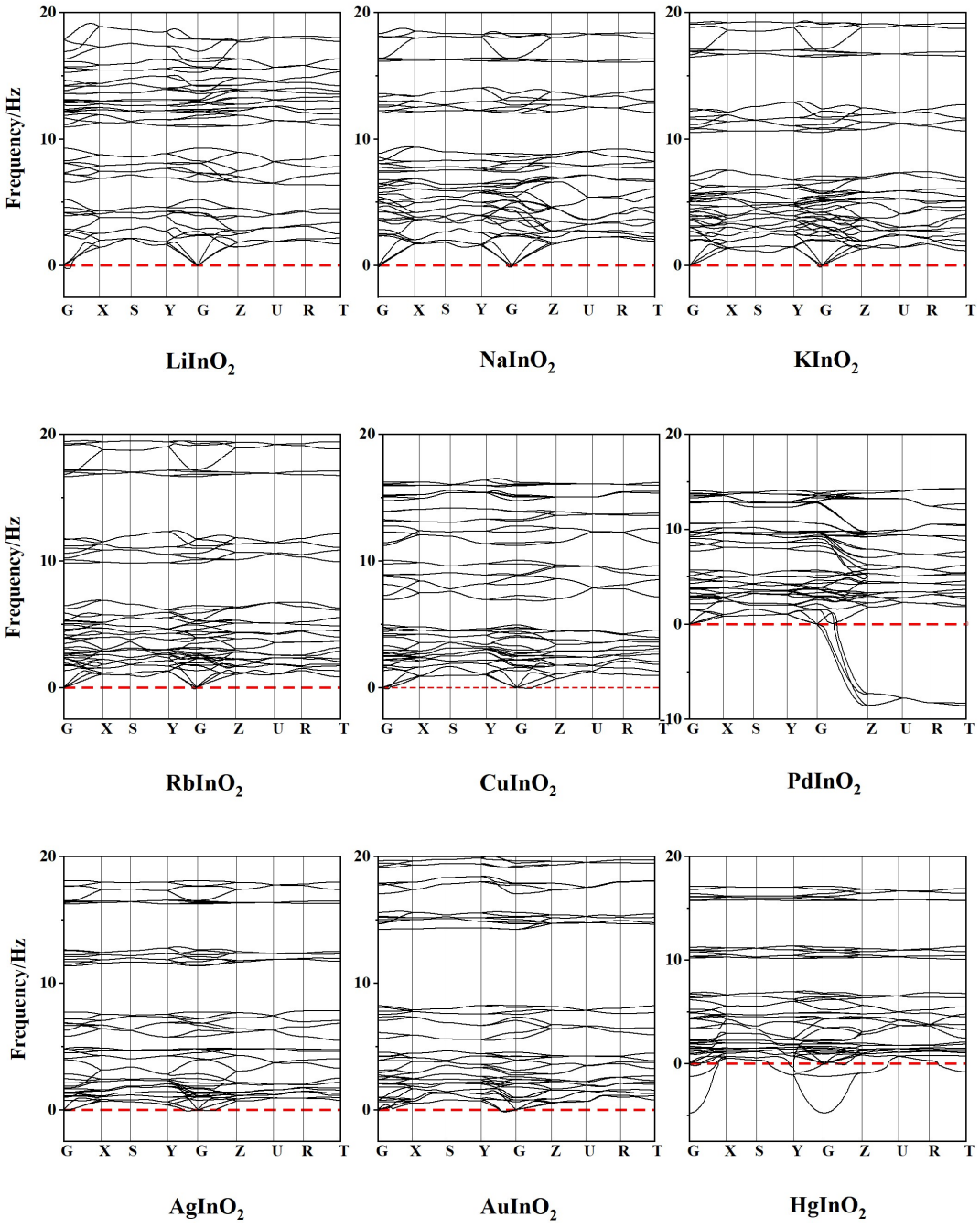

Figure S3 (d). The phonon spectrum of β-$AInO_2$ series system. Among the β-$AInO_2$ oxides, the β-$PdInO_2$ and β-$HgInO_2$ have virtual frequency and are thermodynamically unstable.

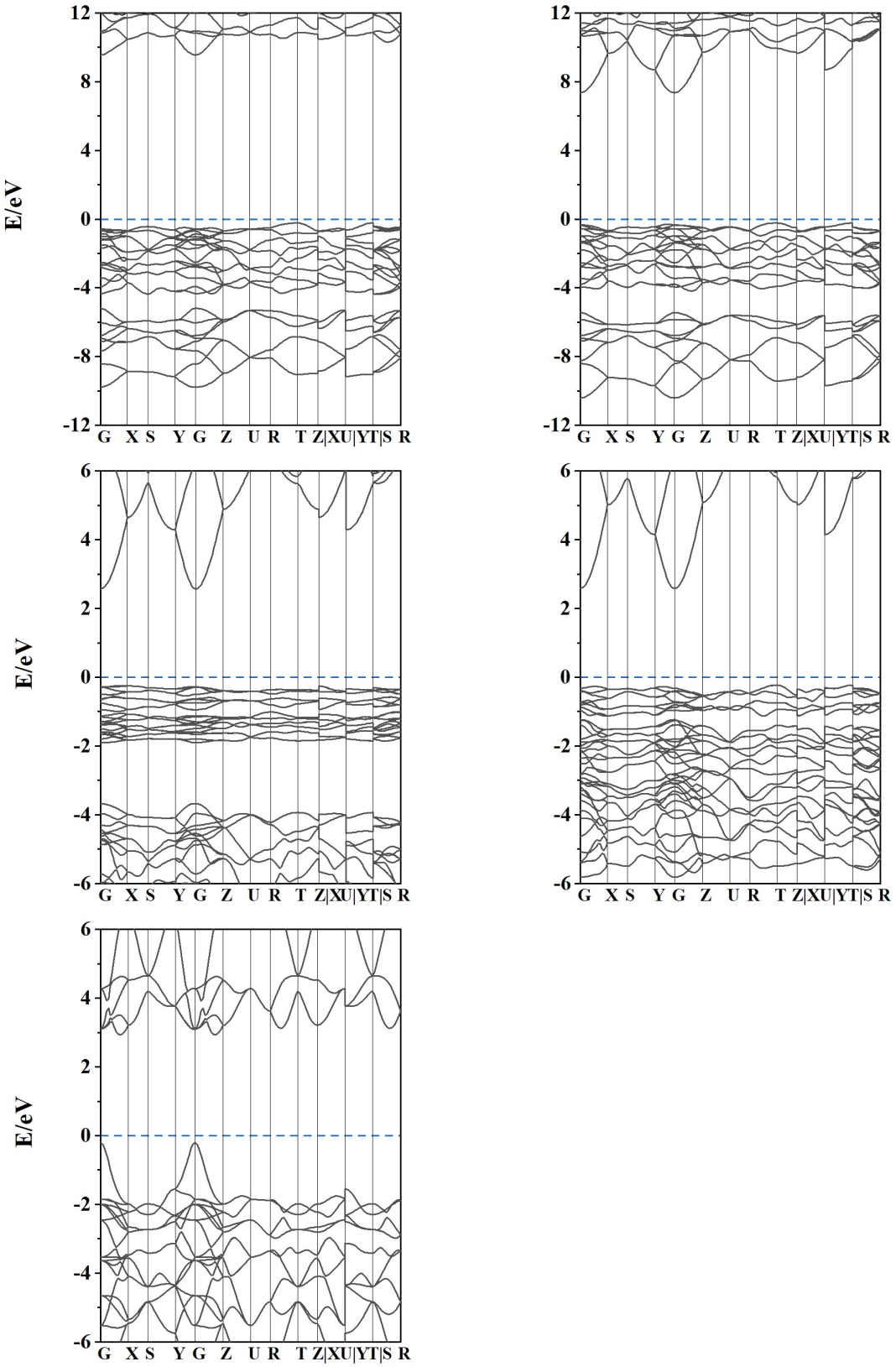

Figure S4 (a). The band structure of β-ABO_2 series system, from left to right: $LiBO_2$, $NaBO_2$, $CuBO_2$, $AgBO_2$, and $TlBO_2$.

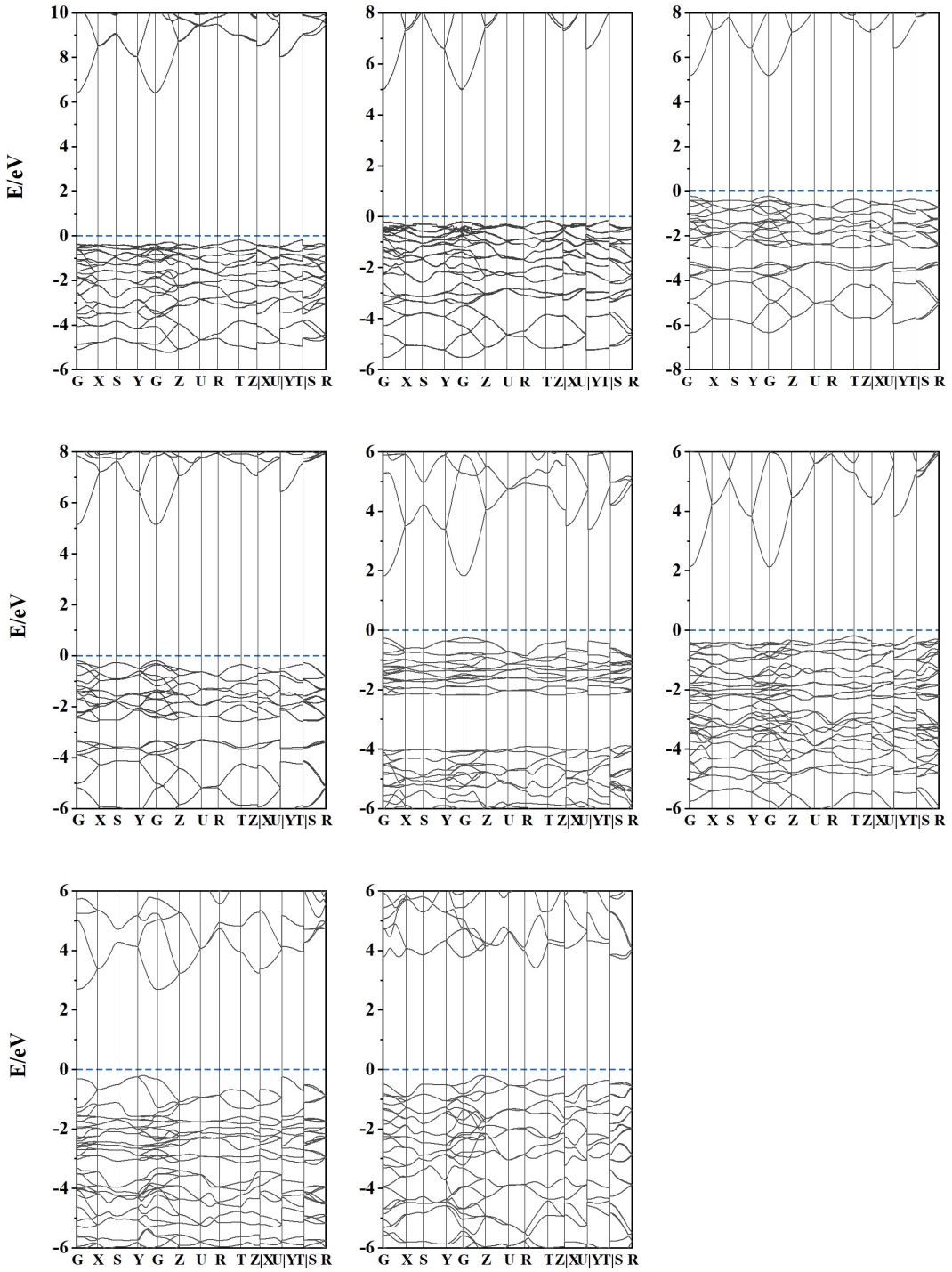

Figure S4 (b). The band structure of β-$AAlO_2$ series system, from left to right: $LiAlO_2$, $NaAlO_2$, $KAlO_2$, $RbAlO_2$, $CuAlO_2$, $AgAlO_2$, $AuAlO_2$, and $TlAlO_2$.

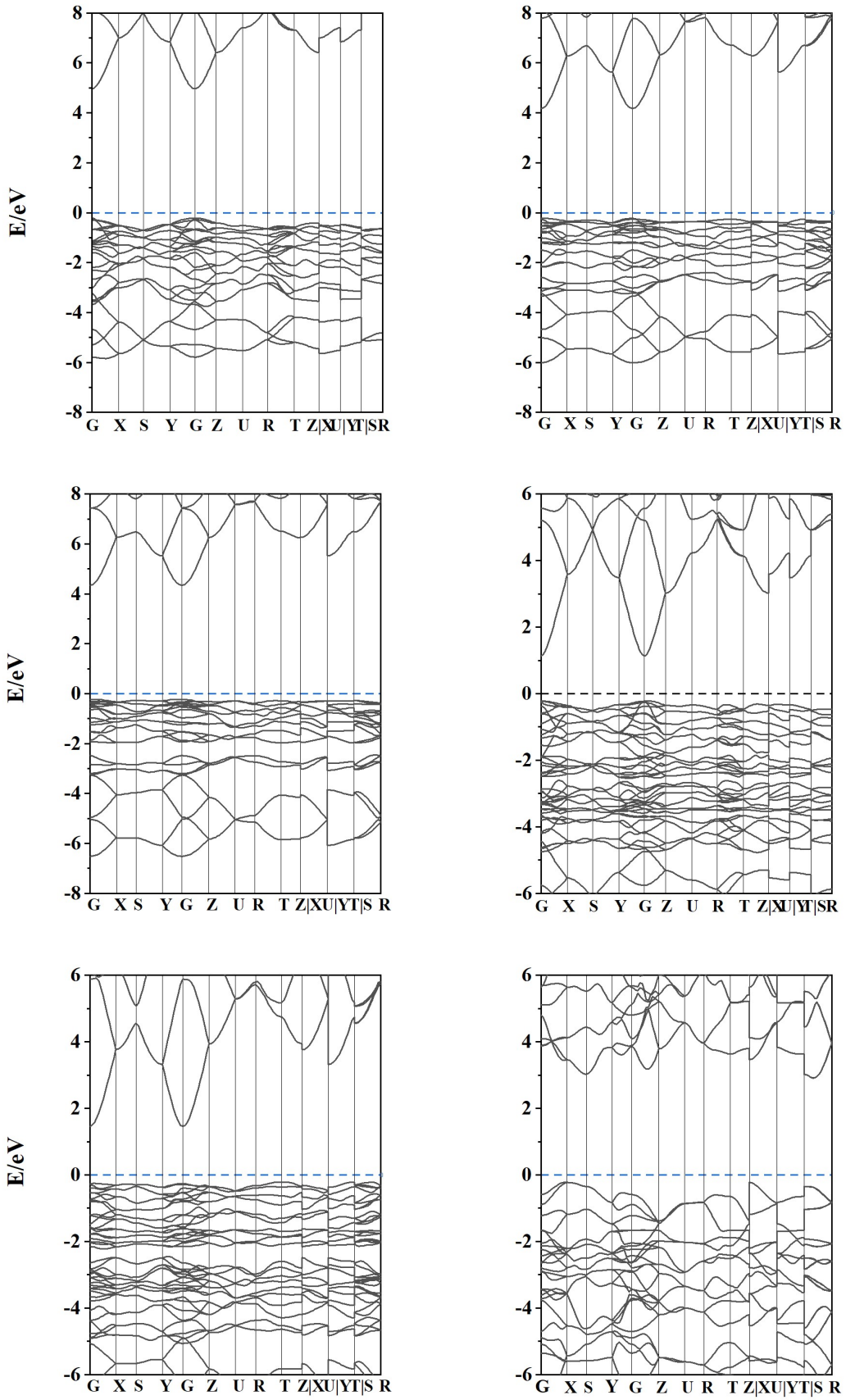

Figure S4 (c). The band structure of β-$AGaO_2$ series system, from left to right: $LiGaO_2$, $NaGaO_2$, $KGaO_2$, $CuGaO_2$, $AgGaO_2$ and $TlGaO_2$.

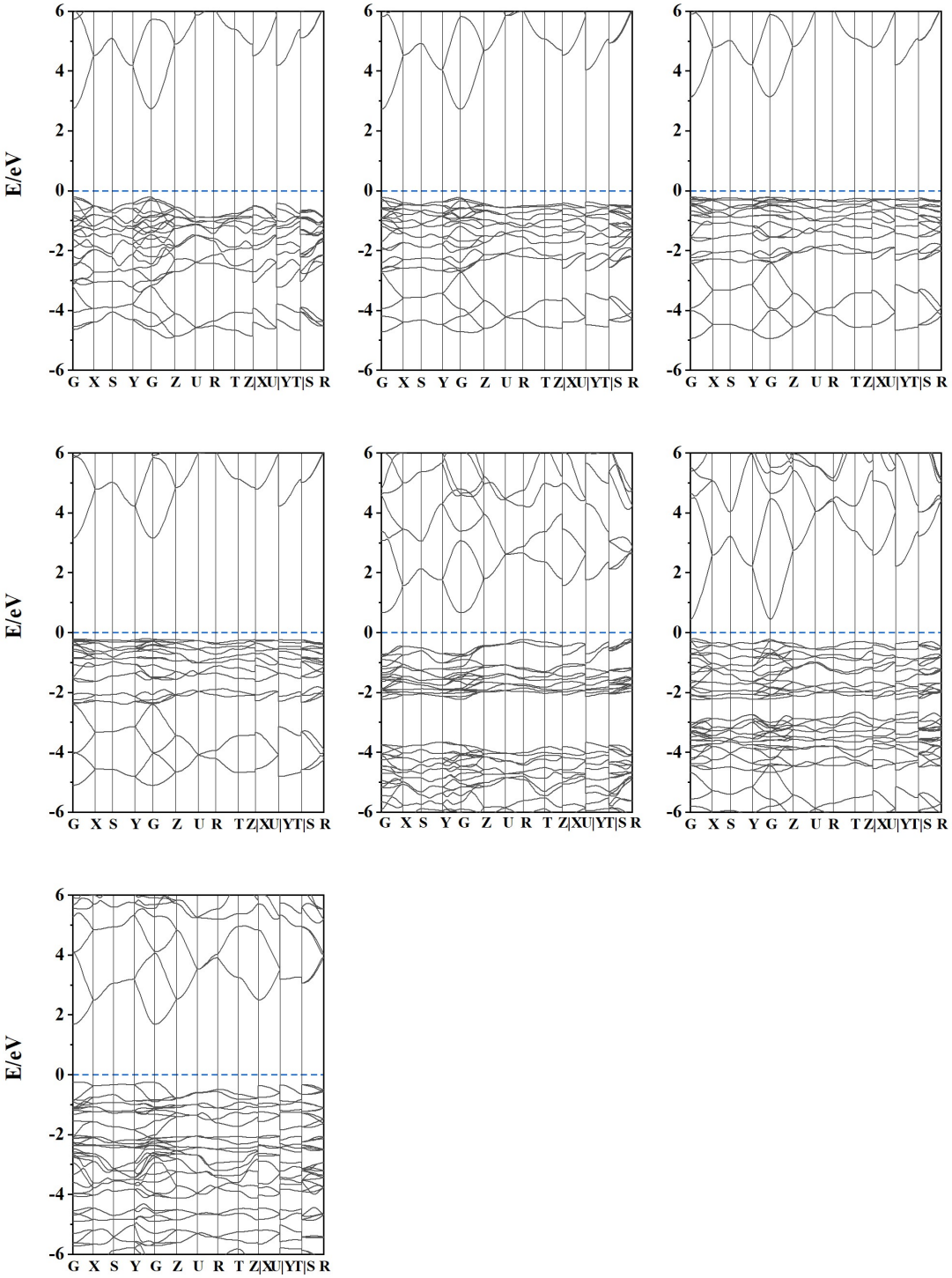

Figure S4 (d). The band structure of β-$AInO_2$ series system, from left to right: $LiInO_2$, $NaInO_2$, $KInO_2$, $RbInO_2$, $CuInO_2$, $AgInO_2$ and $AuInO_2$.

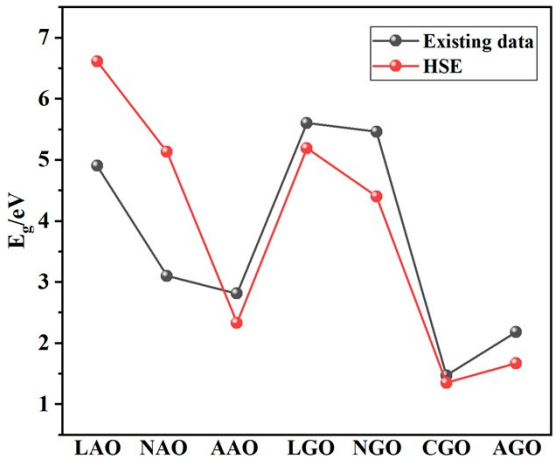

Figure S5. The comparison image of existing band gap data and calculated results. The images show very little difference in the data, proving the reliability of the calculated band gap data.

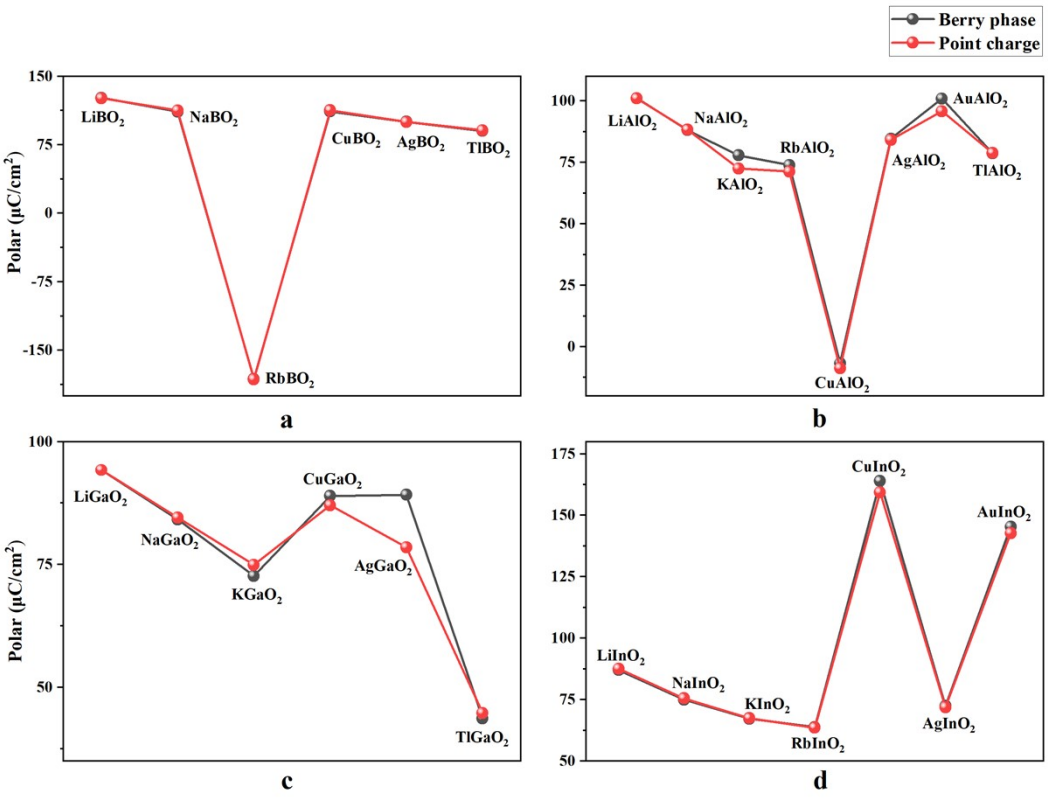

Figure S6. The comparison graph of polarization values obtained by two methods: Berry phase and point-charge method. The images show very little difference in the tow method, proving the reliability of the polarization values.

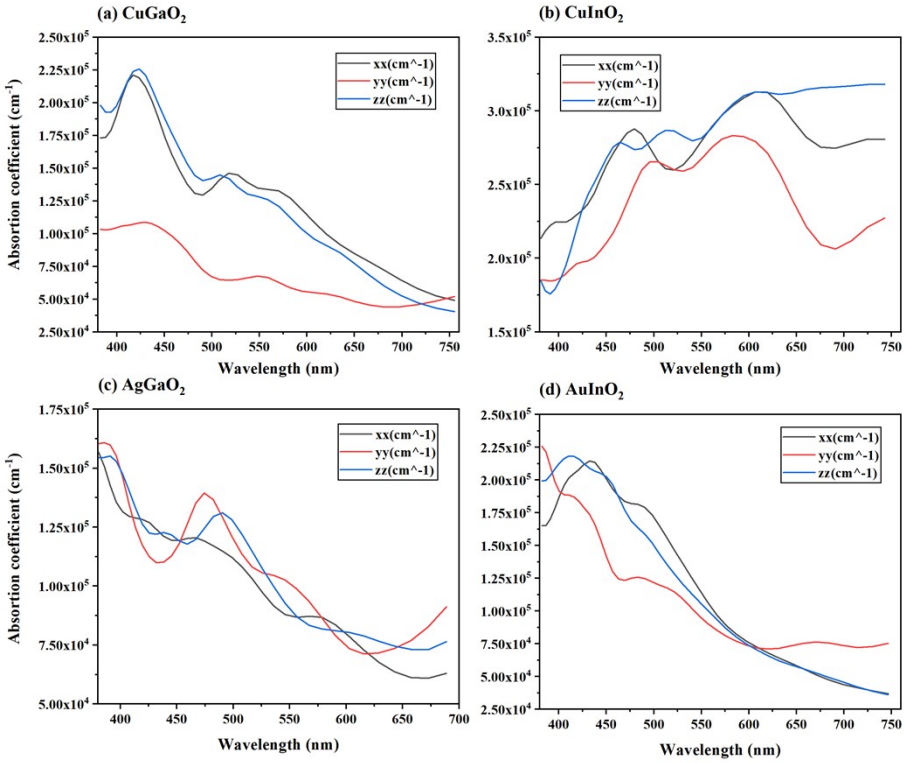

Figure S7. The light absorption spectra of four candidate IFS photocatalysts in three directions (xx, yy and zz).

Table S1. The effective coordination number of A-site and M-site ions.

Coordination number	B		Al		Ga		In	
	AO_x	MO_x	AO_x	MO_x	AO_x	MO_x	AO_x	MO_x
Li	4	4	4	4	4	4	4	4
Na	6	4	4	4	4	4	4	4
K	12	4	4	4	4	4	4	4
Rb	11	4	4	4	5	4	4	4
Cs	9	4	8	4	-	-	-	-
Cu	4	4	3	4	4	4	3	4
Pd	3	4	2	4	2	4	3	4
Ag	6	4	4	4	4	4	4	4
Au	-	-	2	4	2	4	2	4
Hg	-	-	4	4	-	-	4	4
Tl	12	4	6	4	4	4	3	4

The effective number is defined as:

$$ECoN = \sum_i \omega_i \tag{4}$$

where the parameter ω_i is called the bond weight of the ith bond,

$$\omega_i = \exp\left[1 - \left(\frac{l_i}{l_{av}}\right)^6\right] \tag{5}$$

l_{av} is the weighted average bond length

$$l_{av} = \frac{\sum_i l_i \exp\left[1 - (l_i / l_{min})^6\right]}{\sum_i exp\left[1 - (l_i / l_{min})^6\right]} \tag{6}$$

and l_{min} is the smallest bond length in the coordination polyhedron.[4]

Table S2. The calculated bulk modulus B (GPa), shear modulus G (GPa), Young's modulus E (GPa), Poisson's coefficient v

	B				G				E				v			
	B	**Al**	**Ga**	**In**	**B**	**Al**	**Ga**	**In**	**B**	**Al**	**Ga**	**In**	**B**	**Al**	**Ga**	**In**
Li	159.34	92.72	79.45	69.53	121.06	59.74	48.68	26.94	289.78	147.54	121.26	71.57	0.197	0.235	0.246	0.328
Na	147.29	78.40	69.45	62.81	97.01	47.82	36.33	19.92	238.64	119.21	92.81	54.05	0.230	0.247	0.277	0.357
K	-	75.04	67.45	67.78	-	40.42	29.43	13.99	-	102.80	77.07	39.27	-	0.272	0.310	0.403
Rb	151.59	71.56	64.81	68.57	102.83	35.72	27.09	12.30	251.60	91.87	71.32	34.81	0.223	0.286	0.317	0.415
Cs	59.09	90.22	-	-	32.37	55.40	-	-	82.12	137.95	-	-	0.268	0.245	-	-
Cu	173.15	105.80	102.90	51.85	62.13	43.95	38.18	16.41	166.49	115.81	101.92	44.54	0.340	0.318	0.335	0.357
Pd	-	73.13	74.11	-	-	39.63	28.32	-	-	100.70	75.36	-	-	0.271	0.331	-
Ag	190.01	114.67	103.36	90.64	82.85	32.33	20.48	8.94	217.01	88.66	57.64	25.96	0.310	0.371	0.407	0.452
Au	196.68	120.52	-	44.39	51.51	31.58	-	12.42	142.13	87.12	-	34.09	0.380	0.380	-	0.372
Hg	-	97.83	-	-	-	38.62	-	-	-	102.38	-	-	-	0.326	-	-
Tl	160.39	77.55	65.58	-	87.70	39.36	26.81	-	222.53	100.99	70.79	-	0.269	0.283	0.320	-

The bulk modulus (B) can describe the resistance of a material to uniform compression in an elastic system, indicating the bond scalability in crystals. It can be concluded that the average bond strength relationship is β-ABO_2 > β-$AAlO_2$ > β-$AGaO_2$ > β-$AInO_2$.The Young's modulus (E) is defined as the ratio between uniaxial stress and uniaxial deformation within the scope of Hooke's law, which characterizes the stiffness of a material. [5]By comparison, it is found that the stiffness of β-AMO_2 (M=B, Al, Ga, In) materials decreases gradually with the increase of the M-site cation radius, which is consistent with the change of the bond strength. Poisson's ratio (v) is the absolute value of the ratio of transverse positive strain to axial positive strain, which provides some information conducive to the comprehension of the bonding force. [6]The material with large Poisson's ratio indicates that the transverse deformation is larger than the longitudinal deformation when the material is stressed but has no plastic deformation; otherwise, the transverse deformation is smaller than the longitudinal deformation. The upper limit of Poisson's ratio is 0.5, expressing completely incompressible material. In our systems, the magnitude of Poisson's ratio is β-ABO_2 < β-$AAlO_2$ < β-$AGaO_2$ < β-$AInO_2$ < 0.5.

Table S3. The direct and indirect band gap values of stable β-AMO_2 series oxides based on HSE functional.

E_g/eV	E_{in}	E_d	E_g/eV	E_{in}	E_d
$LiBO_2$	9.55	10.12	**$LiAlO_2$**	6.60	6.78
$NaBO_2$	7.58	7.69	**$NaAlO_2$**	5.13	5.18
$CuBO_2$	2.82	2.85	**$KAlO_2$**	-	5.43
$AgBO_2$	2.58	2.90	**$RbAlO_2$**	-	5.37
$TlBO_2$	3.13	3.30	**$CuAlO_2$**	2.09	2.09
			$AgAlO_2$	2.32	2.54
			$AuAlO_2$	2.90	3.02
			$TlAlO_2$	3.62	3.77
E_g/eV	E_{in}	E_d	E_g/eV	E_{in}	E_d
$LiGaO_2$	-	5.19	**$LiInO_2$**	-	2.94
$NaGaO_2$	-	4.40	**$NaInO_2$**	-	2.95
$KGaO_2$	-	4.56	**$KInO_2$**	-	3.36
$CuGaO_2$	-	1.35	**$RbInO_2$**	3.37	3.38
$AgGaO_2$	1.67	1.72	**$CuInO_2$**	0.88	1.39
$TlGaO_2$	3.13	3.28	**$AgInO_2$**	0.66	0.67
			$AuInO_2$	1.93	1.94

Table S4. The hole and electron effective mass of series β-AMO_2 oxides.

	position	m_h/m_0	position	m_e/m_0		position	m_h/m_0	position	m_e/m_0
$LiBO_2$	**R-T**	4.915	**G-X**	2.092	**$LiAlO_2$**	**T-R**	1.356	**G-Z**	0.183
	T-R	1.236	**G-Y**	0.408	**$NaAlO_2$**	**T-R**	0.739	**G-Z**	0.104
	T-S	1.431	**G-Z**	0.361	**$KAlO_2$**	**G-X**	22.553	**G-X**	0.809
$NaBO_2$	**T-R**	1.371	**G-X**	0.729		**G-Y**	1.031	**G-Y**	0.148
	T-G	1.658	**G-Y**	0.161		**G-Z**	1.080	**G-Z**	0.222
			G-Z	0.263	**$RbAlO_2$**	**G-X**	25.025	**G-X**	0.858
$CuBO_2$	**G-X**	5.604	**G-X**	0.786		**G-Y**	0.806	**G-Y**	0.148
			G-Y	0.156		**G-Z**	0.780	**G-Z**	0.201
			G-Z	0.237	**$CuAlO_2$**	**G-Z**	3.518	**G-X**	0.160
$AgBO_2$	**T-R**	1.125	**G-X**	0.630	**$AgAlO_2$**	**T-R**	1.334	**G-Z**	0.157
	T-S	2.472	**G-Y**	0.131	**$AuAlO_2$**	**G-Y**	0.732	**G-X**	1.452
			G-Z	0.222				**G-Y**	0.279
$TlBO_2$	**G-Z**	0.539	**T-R**	0.170				**G-Z**	0.369
					$TlAlO_2$	**G-Z**	0.539	**T-R**	0.170
	position	m_h/m_0	**position**	m_e/m_0		**position**	m_h/m_0	**position**	m_e/m_0
$LiGaO_2$	**G-X**	0.425	**G-X**	0.395	**$LiInO_2$**	**G-X**	3.996	**G-X**	0.897
						G-Y	0.833	**G-Y**	0.135
						G-Z	0.412	**G-Z**	0.187
	G-Y	2.192	**G-Y**	0.206	**$NaInO_2$**	**G-X**	5.631	**G-X**	0.833
$NaGaO_2$	**G-X**	11.052	**G-X**	0.843		**G-Y**	1.526	**G-Y**	0.131
	G-Y	3.609	**G-Y**	0.130		**G-Z**	0.514	**G-Z**	0.183
	G-Z	0.636	**G-Z**	0.191	**$KInO_2$**	**G-X**	13.437	**G-X**	0.832
$KGaO_2$	**G-X**	13.514	**G-X**	0.873		**G-Y**	4.825	**G-Y**	0.139
	G-Y	3.455	**G-Y**	0.132		**G-Z**	2.875	**G-Z**	0.212
	G-Z	2.851	**G-Z**	0.205	**$RbInO_2$**	**G-Y**	1.761	**G-X**	0.841
$CuGaO_2$	**G-X**	5.775	**G-X**	0.235				**G-Y**	0.137
	G-Y	0.886	**G-Y**	0.114				**G-Z**	0.202
$AgGaO_2$	**G-Y**	2.870	**G-X**	0.833	**$CuInO_2$**	**T-R**	0.666	**G-X**	0.947
	G-Z	2.802	**G-Y**	0.108				**G-Y**	0.267
			G-Z	0.127				**G-Z**	0.379
$TlGaO_2$	**G-X**	0.897	**T-R**	0.278	**$AgInO_2$**	**G-X**	1.089	**G-X**	0.967
								G-Y	0.101
								G-Z	0.093
					$AuInO_2$	**G-X**	4.810	**G-X**	1.187
								G-Y	0.208
								G-Z	0.199

Reference

1. Shuxin Ouyang, Haitao Zhang, Dunfang Li, Tao Yu, Jinhua Ye, and Zhigang Zou, 2006.
2. M. Parrinello and A. Rahman, *The Journal of Chemical Physics*, 1982, **76**, 2662-2666.
3. S. F. Pugh, *The London, Edinburgh, and Dublin Philosophical Magazine and Journal of Science*, 2009, **45**, 823-843.
4. K. Momma and F. Izumi, *Journal of Applied Crystallography*, 2011, **44**, 1272-1276.
5. L. Guo, S. Zhu, S. Zhang and W. Feng, *Computational Materials Science*, 2014, **92**, 92-101.
6. N. I. Christensen, *Journal of Geophysical Research: Solid Earth*, 1996, **101**, 3139-3156.